NANO LETTERS

pubs.acs.org/NanoLett Letter

Confined Flash Pt_1/WC_x inside Carbon Nanotubes for Efficient and Durable Electrocatalysis

Sheng Zhu,* Qian Xu, Chong Guan, Yunzhen Chang, Gaoyi Han, and Bing Deng*

Cite This: https://doi.org/10.1021/acs.nanolett.4c05097 Read Online

ACCESS | Metrics & More | Article Recommendations | Supporting Information

ABSTRACT: Exploiting cost-effective hydrogen evolution reaction (HER) catalysts is crucial for sustainable hydrogen production. However, currently reported nanocatalysts usually cannot simultaneously sustain high catalytic activity and long-term durability. Here, we report the efficient synthesis and activity tailoring of a chainmail catalyst, isolated platinum atom anchored tungsten carbide nanocrystals encapsulated inside carbon nanotubes (Pt_1/WC_x@CNTs), by confined flash Joule heating technique. The instantaneous carbothermal reduction reaction enables the millisecond formation of Pt_1/WC_x nanostructures from CNT-encapsulated polyoxometalates, where nanotubes serve as both heating conductors and robust chainmails. The Pt_1/WC_x@CNTs exhibit prominent catalytic performance toward acid HER with a low overpotential of 45.2 mV at 10 mA cm^{-2} and long-term durability over 500 h of continuous running. Mechanism studies reveal the strong metal−support interaction on Pt_1/WC_x optimizes the charge redistribution at the Pt_1-W_2C interface and the hydrogen adsorption/desorption behavior. This study offers a potential avenue for ultrafast and activity-controllable synthesis of highly stable single-atom catalysts.

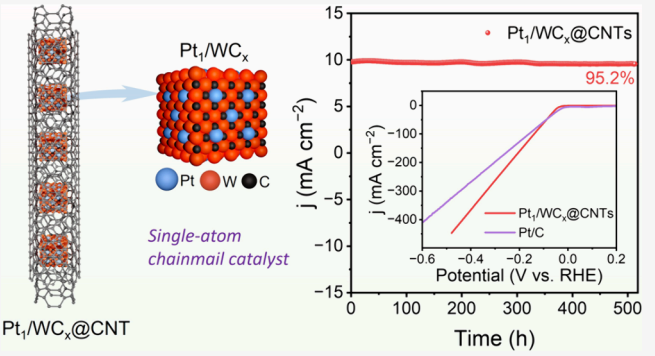

KEYWORDS: *Flash Joule heating, hydrogen evolution, single-atom catalysis, carbon nanotubes, confinement, tungsten carbide*

Hydrogen energy is regarded as a promising clean energy source, and has the potential to address the energy concern caused by excessive consumption of fossil fuels.[1−5] In recent years, the electrochemical hydrogen evolution reaction (HER), which can produce hydrogen from water in an efficient and environmentally sustainable way, has aroused extensive research interest.[6−8] At present, one of the main challenges faced by HER is the slow reaction kinetics; hence, highly active and robust electrocatalysts are indispensable.[9−11] Noble metal platinum (Pt) is regarded as the benchmark catalyst for HER owing to its unique electronic structure and optimal binding energy with hydrogen. However, the scarcity and high cost of Pt limit its broader application.[12−15] In recent years, considerable efforts have been devoted to exploit promising alternatives of conventional platinum-based catalysts.[9,16] One strategy is to prepare nonprecious metal based HER catalysts, such as Fe, Ni, W, Mo, etc.,[17−20] whereas these catalysts often suffer from degradation of catalytic activity and durability during long-term operation. Another approach is to reduce the Pt content by using alloy catalysts or single atom catalysts (SACs).[21−25] So far, atomic Pt species have been immobilized on various carriers such as carbon nanostructures and transition metal oxides/sulfides/phosphides/carbides with appropriate metal−support interactions to form SACs.[26−31] The single Pt center can bond with adjacent atoms to help regulate local geometrical/electronic configurations, thereby achieving comparable catalytic performance to bulk Pt catalyst.[32−34]

Among various SAC carriers, tungsten carbides have been widely investigated as their *d*-band electronic states are similar to Pt-group materials.[35,36] For instance, Li et al. reported WC_x-FeNi as a kind of highly efficient catalyst for oxygen evolution reaction, in which WC_x were employed to stabilize atomic or biatomic metals (Fe, Ni, or FeNi).[37] Recently, Lin et al. synthesized a Ru SAs/WC_x catalyst where atomical Ru atoms were anchored on the surface of tungsten carbide nanocrystallites.[38] Ru was proved to alleviate OH blocking and boost alkaline HER activity by the strong puncture effect. These advances demonstrate the feasibility and efficiency of tungsten carbides as SAC carriers for high performance electrocatalysts. Despite all this, the preparation of these catalysts typically involves a long period of pyrolysis, the individual metal atoms are easy to aggregate into clusters or nanoparticles and thus, impeding the large-scale production

Received: October 14, 2024
Revised: December 24, 2024
Accepted: December 26, 2024

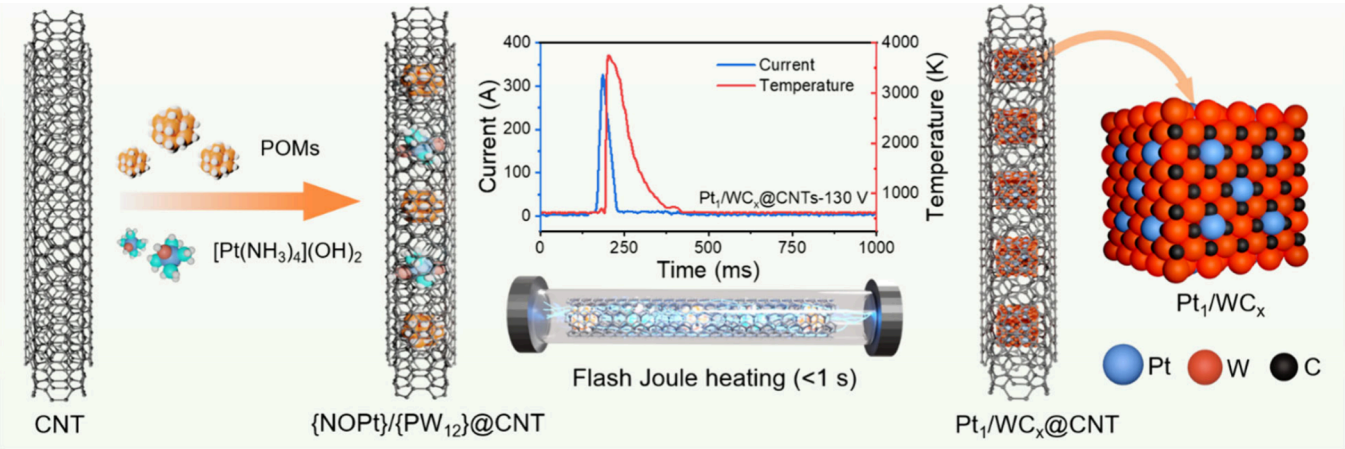

Figure 1. Schematic diagram for synthesis of the Pt_1/WC_x@CNT catalyst by the CFJH technique.

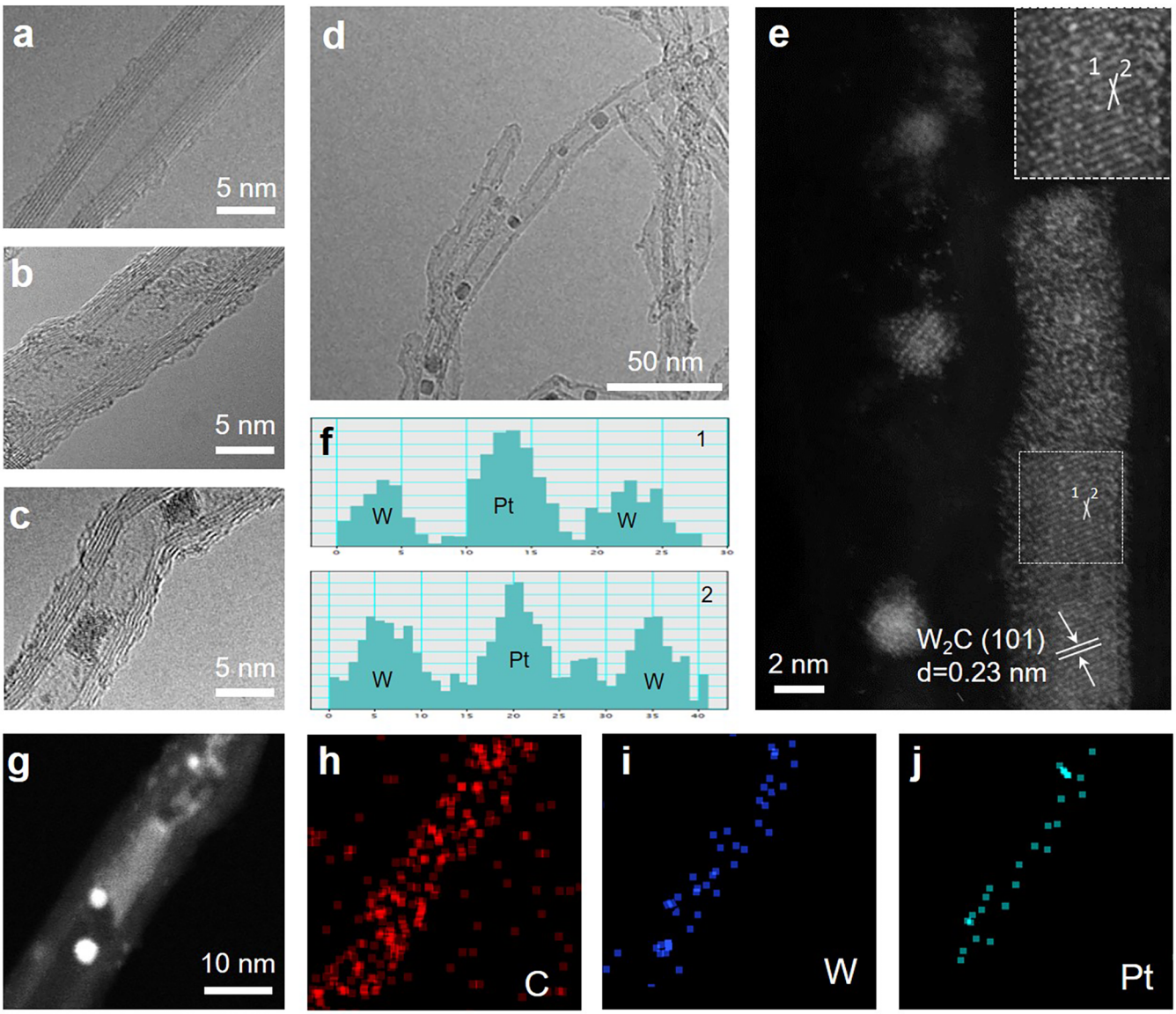

Figure 2. Micromorphology of the Pt_1/WC_x@CNTs. HRTEM images of CNTs (a), {NOPt}/{PW_{12}}@CNTs (b), and Pt_1/WC_x@CNTs (c, d). (e) AC-HADDF-STEM image of Pt_1/WC_x@CNTs. (f) Intensity analysis of line profiles 1 and 2 in (e). HADDF-STEM image (g) and corresponding elemental mapping images (h−j) of Pt_1/WC_x@CNTs.

https://doi.org/10.1021/acs.nanolett.4c05097
Nano Lett. XXXX, XXX, XXX−XXX

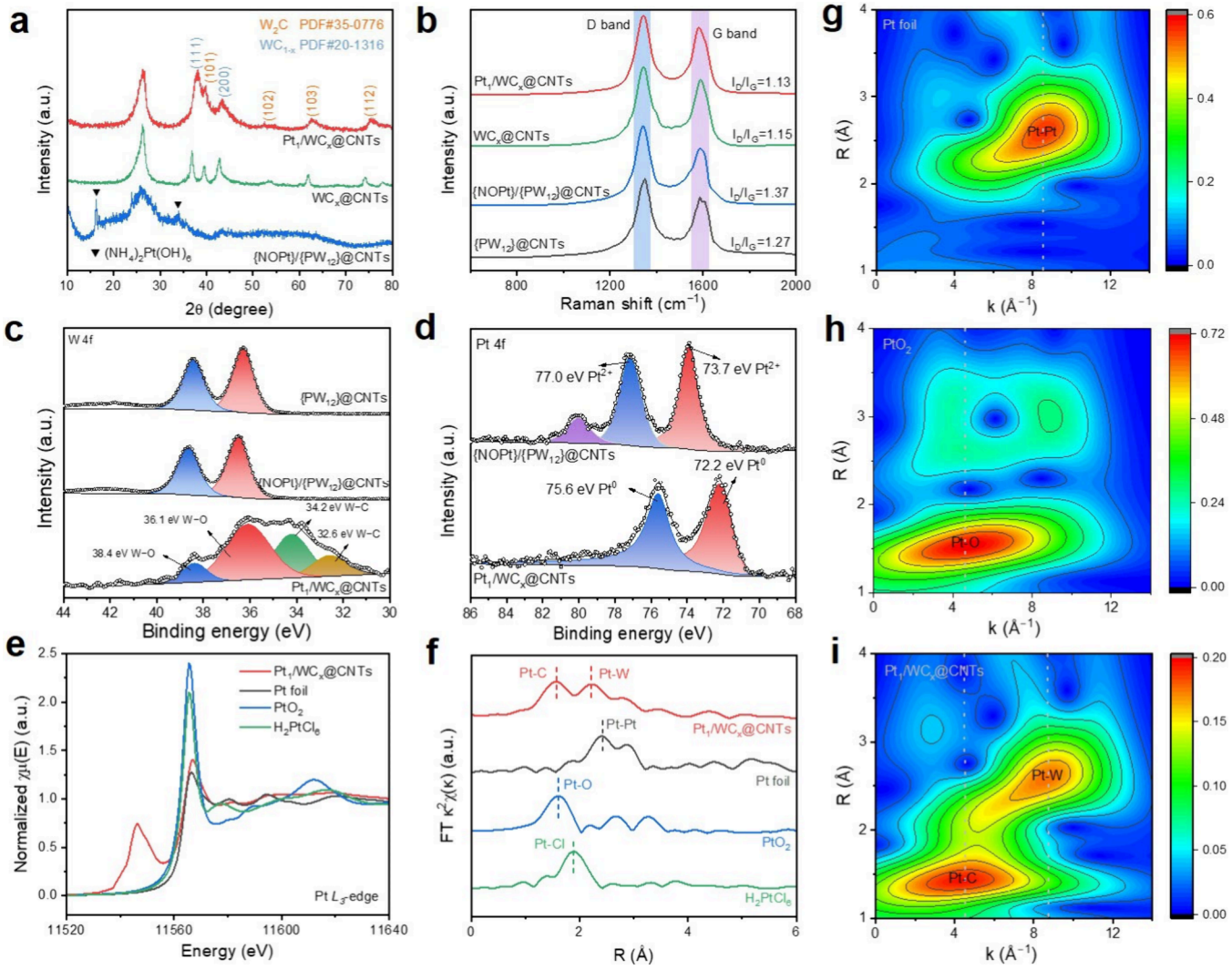

Figure 3. Fine structure of Pt_1/WC_x@CNTs. (a) XRD pattern of Pt_1/WC_x@CNTs, WC_x@CNTs, and {NOPt}/{PW_{12}}@CNTs. The PDF references are W_2C, PDF#35−0776, and WC_{1-x}, PDF#20−1316. (b) Raman spectra of {PW_{12}}@CNTs, {NOPt}/{PW_{12}}@CNTs, WC_x@CNTs, and Pt_1/WC_x@CNTs. The blue and purple shadows depict the D and G bands, respectively. (c) XPS fine spectra of W 4f in {PW_{12}}@CNTs, {NOPt}/{PW_{12}}@CNTs, and Pt_1/WC_x@CNTs. (d) XPS fine spectra of Pt 4f in {NOPt}/{PW_{12}}@CNTs and Pt_1/WC_x@CNTs. Pt L_3-edge XANES spectra (e) and k^2-weighted FT-EXAFS spectra (f) of Pt_1/WC_x@CNTs, Pt foil, PtO_2, and H_2PtCl_6. The WT-EXAFS images were of Pt foil (g), PtO_2 (h), and Pt_1/WC_x@CNTs (i).

and application of WC_x-based SACs. On another hand, previous studies have revealed that exposed W carbide nanocrystallites are unstable and tend to react with H_2O to form W oxides.[39] This would cause both structure and activity degradation of prepared SACs during continuous operation in aqueous media. Therefore, it is of great importance to design and construction of highly active and robust WC_x-based SACs, whereas it remains a serious challenge.

As an emerging ultrafast synthesis method, Joule heating technique has received tremendous interests for the rational preparation of nanomaterials in a controllable, eco-friendly, and scalable way.[40,41] Herein, we report the ultrafast confined synthesis of Pt_1/WC_x nanostructures inside multiwalled carbon nanotubes (MWCNTs) via confined flash Joule heating (CFJH) technique, forming Pt_1/WC_x@CNT chainmail catalyst. The well-defined WC_x carriers are converted from the polyoxometalate (POM) clusters inside nanotubes through an instantaneous carbothermal reduction reaction in less than 1 s, accompanied by the incorporation of isolated Pt atoms in the carbide framework. The Pt content and CFJH parameters are optimized to achieve the millisecond modulation of the HER catalytic performance. Impressively, the optimal Pt_1/WC_x@CNT catalyst exhibits prominent HER performance with high catalytic/mass activity, rapid reaction kinetics, and long-term durability, superior to that of commercial Pt/C catalyst.

Catalyst Synthesis. Figure 1 depicts the synthesis schematic of the Pt_1/WC_x@CNT chain-mail catalyst based on the CFJH technology. First, a certain amount of MWCNTs, tetraammonium platinum hydroxide ($H_{14}N_4O_2Pt{\cdot}xH_2O$, denoted as {NOPt}), and phosphotungstic acid hydrate ($H_3O_{40}PW_{12}{\cdot}xH_2O$, denoted as {$PW_{12}$}) are assembled into the catalyst precursors of {NOPt}/{PW_{12}}@CNTs, where {NOPt} and {PW_{12}} molecules are encapsulated inside the nanotube cavities via a mild host−guest chemistry strategy.[42] The infrared spectra of these samples are shown in Figure S1. Subsequently, the WC_x crystals are converted from {PW_{12}} clusters inside MWCNTs through a highly efficient carbothermal reduction reaction, accompanied by the anchoring of

https://doi.org/10.1021/acs.nanolett.4c05097
Nano Lett. XXXX, XXX, XXX−XXX

individual Pt atoms within the carbide framework. The entire CFJH process is free of any solvents and special gases, and completed with carbon nanotubes as both templates and heating conductors. During the reaction, a high current pulse up to 326 A brings the sample temperature up to 3700 K at a discharge voltage of 130 V, which then rapidly drop to room temperature within 500 ms. Based on thermogravimetric analyses (Figure S2), the encapsulation efficiency of Pt_1/WC_x inside CNTs is determined as ~23.5%.

According to the scanning electron microscopy (SEM) image (Figure S3) and high-resolution transmission electron microscopy (HRTEM) image (Figure 2a), MWCNTs have the diameter of 5−10 nm with few sidewalls (less than 10 layers). After decorating {NOPt} and $\{PW_{12}\}$ molecules, the dark dots inside the nanotubes are clearly visible (Figure 2b). The subsequent CFJH treatment enables the ultrafast conversion of $\{NOPt\}/\{PW_{12}\}$ into Pt_1/WC_x nanostructures in MWCNTs. The CNTs-encapsulated Pt_1/WC_x nanostructures have the particle size of 2−5 nm (Figure 2c, d), which is largely dependent on the inner diameter of nanotubes, demonstrating the well-defined encapsulation of these nanostructures within nanotubes.

The existence form of Pt species is further examined by aberration-corrected high-angle annular dark-field scanning transmission electron microscopy (AC-HAADF-STEM). Many individual bright spots are visible within the crystal framework of carbides (Figure 2e), indicating the atomical dispersion of Pt. The lattice spacing of 0.23 nm can be ascribed to the (101) crystal plane of W_2C with a hexagonal phase. Some regions of the carbides present an amorphous structure, which maybe due to the ultrahigh cooling rate ($>10^4$ K s^{-1}) during the CFJH process. It has a major effect on the formation of crystal or glassy phases.[43] The intensity profiles in Figure 2e indicate that Pt atoms partially replace W sites in the WC_x carrier (Figure 2f). Energy-dispersive X-ray spectroscopy (EDS) elemental mapping images show the inner dispersion of W and Pt elements inside the MWCNTs and an even distribution of Pt over the WC_x carriers (Figures 2g−j).

Catalyst Characterization. Extensive characterizations were performed to depict the composition and structure of the Pt_1/WC_x@CNTs. First, X-ray diffraction (XRD) was conducted to unveil the structure evolution during the CFJH synthesis (Figure 3a). Two detectable diffraction peaks at 2θ = 16.1° and 33.8° are ascribed to $(NH_4)_2Pt(OH)_6$ inside the nanotubes. After the CFJH reaction, the signals of $(NH_4)_2Pt(OH)_6$ disappear, accompanied by the formation of WC_x peaks. The encapsulated tungsten carbides are composed of binary phases, including hexagonal W_2C and cubic WC_{1-x}.[36,44,45] No characteristic signals of metallic Pt are observed, further implying that Pt species are atomically dispersed in the carbide crystals. Without the addition of $(NH_4)_2Pt(OH)_6$, the synthesized WC_x@CNT hybrid shows a similar XRD profile as that of Pt_1/WC_x@CNTs, proving that the incorporation of isolated Pt atoms does not change the crystal phase of tungsten carbides.

Figure 3b presents the Raman spectra of $\{PW_{12}\}$@CNTs, $\{NOPt\}/\{PW_{12}\}$@CNTs, as well as their derived WC_x@CNTs and Pt_1/WC_x@CNTs after CFJH. The intensity ratio of the D band at ~1350 cm^{-1} to the G band at ~1590 cm^{-1} (I_D/I_G) is employed to assess structure defects of carbon materials. The confined carbides are formed through the carbothermal reduction reaction between $\{PW_{12}\}$ molecules with nanotubes. This process would lead to the formation of structure defects for MWCNTs. Interestingly, the I_D/I_G values of Pt_1/WC_x@CNTs and WC_x@CNTs are lower than those of $\{NOPt\}/\{PW_{12}\}$@CNTs and $\{PW_{12}\}$@CNTs, respectively. This is probably attributed to the high instantaneous temperature of CFJH technique that is capable of repairing the CNT defects (Figure S7).[46] XPS fine spectra of W 4f in different samples are presented in Figure 3c. The two peaks at 32.6 and 34.2 eV of Pt_1/WC_x@CNTs ascribe to the W $4f_{7/2}$ and W $4f_{5/2}$ of W−C bond, while the peaks with higher binding energies of 36.1 and 38.4 eV are assigned to the W $4f_{7/2}$ and W $4f_{5/2}$ of W−O bond, originating from the partial surface oxidation of nanosized tungsten carbide.[36] Then, for Pt, the XPS fine spectra of Pt 4f in $\{NOPt\}/\{PW_{12}\}$@CNTs can be deconvoluted into two peaks at 73.7 and 77.0 eV, which are assigned to the Pt $4f_{7/2}$ and Pt $4f_{5/2}$ states of Pt^{2+}, respectively (Figure 3d). A peak at ~80 eV may be attributed to the Pt species with high valence state.[47] Noteworthy, we observe two distinctive peaks at 72.2 and 75.6 eV for Pt_1/WC_x@CNTs, indicating that the valence state of atomically dispersed Pt species is close to zero.[48]

The localized electronic structure and coordination environment of Pt_1/WC_x@CNTs were further determined by the X-ray absorption near-edge structure (XANES) and extended X-ray absorption fine structure (EXAFS). As depicted in Figure 3e, a prepeak arisen in XANES curve of the Pt_1/WC_x@CNTs can be due to the nonplanar configuration of Pt species in the WC_x lattice.[31] The near-edge absorption of Pt_1/WC_x@CNTs is located between H_2PtCl_6 and Pt foil and closer to Pt foil, confirming the average valence state of isolated Pt atoms approaches to zero. This analysis is consistent with the XPS results mentioned above. The R-space curve of Fourier-transformed (FT) k^2-weighted extended X-ray absorption fine structure (EXAFS) of the Pt_1/WC_x@CNTs is displayed in Figure 3f. The R-space fine spectrum of H_2PtCl_6 exhibits a strong peak at around 1.9 Å, which is attributed to the Pt−Cl bond. In addition, there is a prominent peak of Pt−O at 1.6 Å for PtO_2, and Pt−Pt at 2.4 Å for the Pt foil.[49] Notably, we find two distinct coordination peaks at 1.6 and 2.2 Å for Pt_1/WC_x@CNTs, which are attributed to Pt−C and Pt−W bonds, respectively.[50,51] No visible Pt−Cl or Pt−Pt signals are detected, signifying the stabilization of isolated Pt atoms in the WC_x framework. Figure 3g−i depicts the wavelet-transform EXAFS (WT-EXAFS) analyses of Pt foil, PtO_2, and Pt_1/WC_x@CNTs. From the contour images, Pt_1/WC_x@CNT shows the maximum intensity at ~4.5 $Å^{-1}$ (Pt−C) and a second maximum at ~8.7 $Å^{-1}$ (Pt−W), different from the Pt foil (~8.5 $Å^{-1}$, Pt−Pt) and PtO_2 (~4.6 $Å^{-1}$, Pt−O).[52] These results explicitly prove that Pt atoms are anchored in the carbide substrate and coordinated with C (first shell) and W (second shell) atoms to form SACs.

Structure Modulation and Electrocatalytic Activity. The rapid synthesis capability of CFJH enables the precise tunability of Pt_1/WC_x@CNT structures, which have been controlled by changing the CFJH voltages (Figures S9−S13). The linear sweep voltammetry (LSV) polarization curves and Tafel plots are depicted in Figure S14. The Nyquist plots in Figure S15 indicate the favorable HER kinetics of Pt_1/WC_x@CNT-130 V with low charge transfer resistance (R_{ct}). Furthermore, the double layer capacitance (C_{dl}) is determined from the cyclic voltammetry (CV) curves (Figure S16), and Pt_1/WC_x@CNT-130 V presents the highest C_{dl} value of 13.1 mF cm^{-2}, implying the highest number of active centers. Its overall performances are compared with those of the reported acidic HER catalysts (Figure S17 and Table S1).

https://doi.org/10.1021/acs.nanolett.4c05097
Nano Lett. XXXX, XXX, XXX−XXX

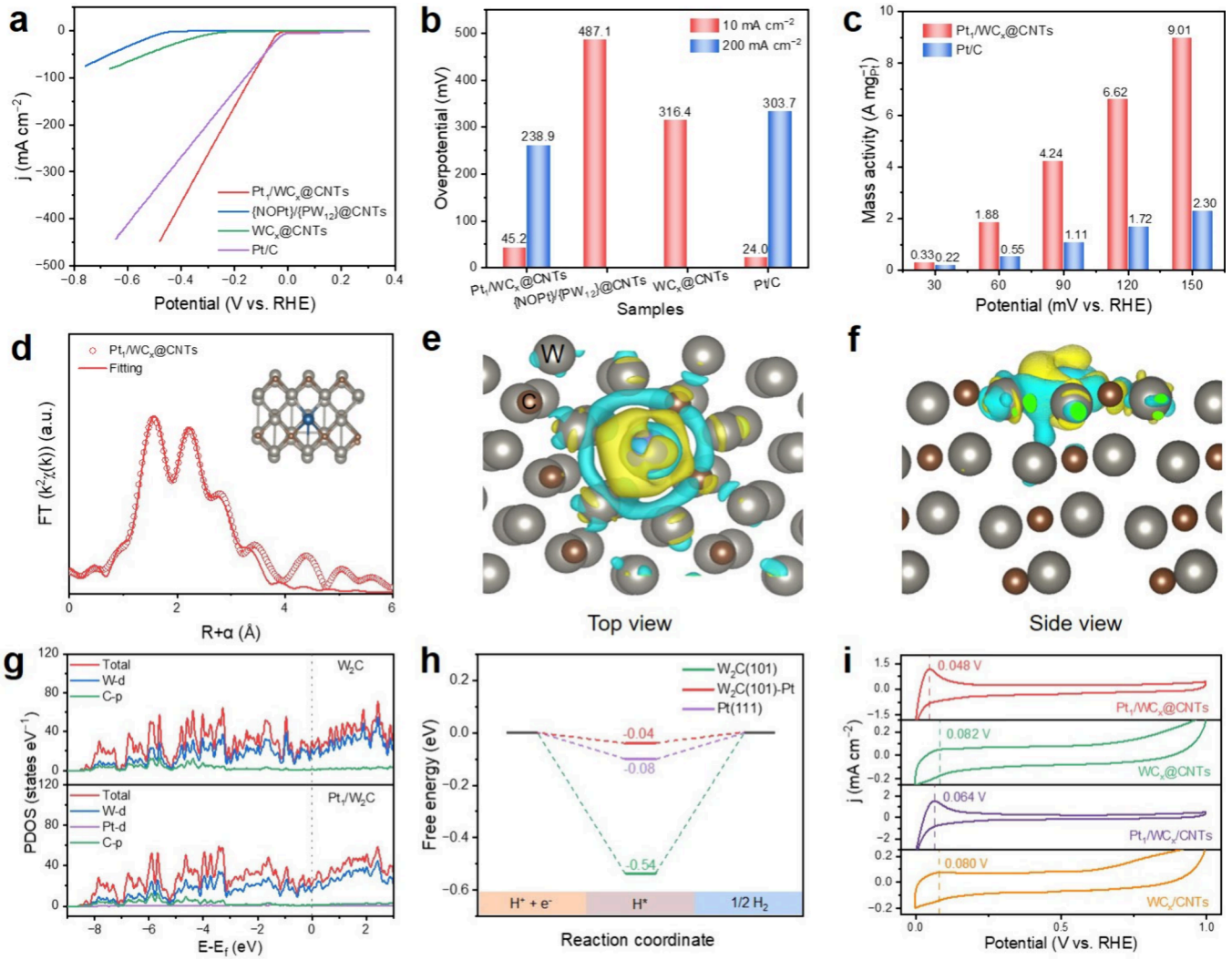

Figure 4. HER performance and theoretical investigation. (a) HER LSV polarization curves at a scan rate of 10 mV s^{-1}. (b) Overpotential at the current density of 10 and 200 mA cm^{-2}. (c) Mass activity of Pt$_1$/WC$_x$@CNTs in comparison with 20 wt % Pt/C. (d) Fitting curve of the k^2-weighted Pt L$_3$-edge EAXFS spectrum for Pt$_1$/WC$_x$@CNTs. Inset: model of the local coordination structure. Top view (e) and side view (f) images of Pt$_1$/W$_2$C with different charge density; the yellow and cyan regions represent charge accumulation and charge depletion, respectively. (g) PDOS of W$_2$C and Pt$_1$/W$_2$C, with aligned Fermi level. (h) Calculated Gibbs free energy for H* adsorption on W$_2$C, Pt$_1$/W$_2$C, and Pt. (i) CV curves of Pt$_1$/WC$_x$@CNTs, WC$_x$@CNTs, Pt$_1$/WC$_x$/CNTs, and WC$_x$/CNTs in N$_2$-saturated 0.5 M H$_2$SO$_4$ medium.

According to the above analyses, Pt$_1$/WC$_x$@CNT obtained at 130 V shows the best HER performances, and thus, it is further tested and compared with the commercial Pt/C benchmark. The LSV polarization curves and corresponding overpotentials are shown in Figure 4a,b. The overpotentials of Pt$_1$/WC$_x$@CNTs are 45.2 and 238.9 mV under the current densities of 10 and 200 mA cm^{-2}, respectively, significantly superior over WC$_x$@CNTs, indicating the important role of isolated Pt atoms in HER. The Tafel slope of Pt$_1$/WC$_x$@CNT catalyst (38.0 mV dec^{-1}) is much lower than the commercial Pt/C and other catalysts, implying the fast HER kinetics (Figure S18). Pt$_1$/WC$_x$@CNTs exhibits a lower R_{ct} value of 4.8 Ω than WC$_x$@CNTs (16.5 Ω, Figure S19), evidencing a strong interaction between Pt atoms and carbide supports, which leads to faster charge transfer at the catalyst/electrolyte interface.[49] The CV curves of different samples are shown in Figure S20, and Pt$_1$/WC$_x$@CNT has the largest C_{dl} value, indicating the highest electrochemical active surface area and abundant active sites.

We also prepared a series of catalysts to investigate the effect of Pt loading on the electrochemical performance of the catalysts (Figures S21−S26). These findings suggest that the optimal catalytic activity is achieved when the {NOPt} dosage is 30 mg. The mass activity and turnover frequency (TOF) of the optimal Pt$_1$/WC$_x$@CNT catalyst are analyzed (Table S2, Figures 4c, S27−S29). Our Pt$_1$/WC$_x$@CNT catalyst achieves a mass activity of 9.01 A mg$_{Pt}^{-1}$ at 150 mV, which is ∼3.9 times higher than that of the 20 wt % Pt/C benchmark (MA_{150} = 2.30 A mg$_{Pt}^{-1}$). Furthermore, it presents a higher TOF value (5.06 H$_2$ s^{-1}) at 100 mV than the Pt/C catalyst (1.33 H$_2$ s^{-1}). These results clearly demonstrate the high intrinsic catalytic activity of the Pt$_1$/WC$_x$@CNTs in an acidic HER.

Mechanism and Structure−Activity Relationship. To elucidate the mechanism of the electrocatalytic activity of the single-site Pt$_1$/W$_2$C nanostructure, density functional theory (DFT) calculation was conducted to further clarify the metal−support interactions. First, based on the AC-HADDF-STEM and XRD results, we employed the (101) crystal plane of W$_2$C as the basic model for WC$_x$ and Pt$_1$/WC$_x$. Then, based on

https://doi.org/10.1021/acs.nanolett.4c05097
Nano Lett. XXXX, XXX, XXX−XXX

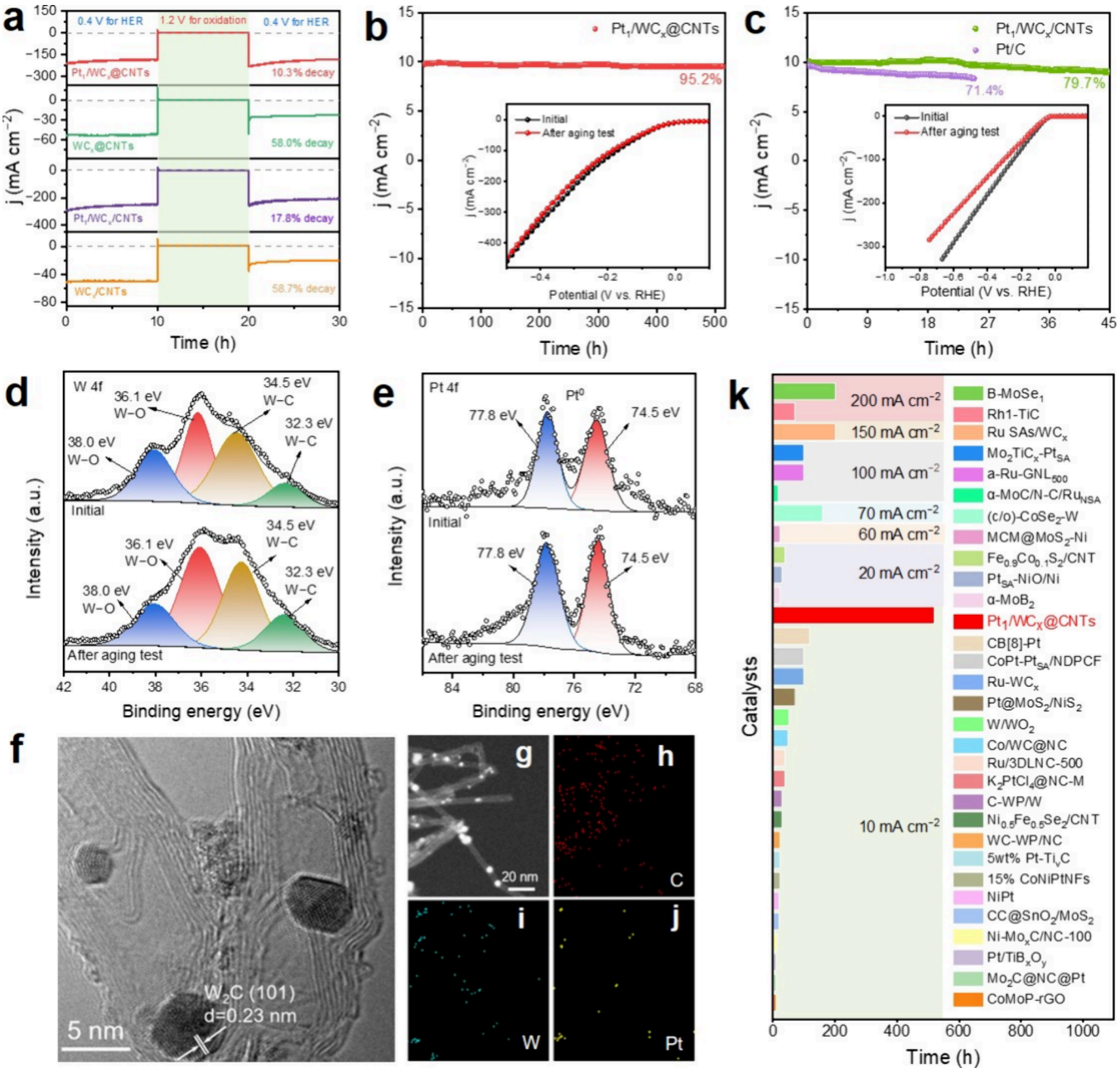

Figure 5. Long-term durability of structure and HER performance. (a) Oxidative decay of Pt_1/WC_x@CNTs, WC_x@CNTs, Pt_1/WC_x/CNTs, and WC_x/CNTs after an oxidation potential of 1.2 V for 10 min. (b) Long-term HER stability test of Pt_1/WC_x@CNTs. Inset: LSV polarization curves before and after aging test. (c) Long-term HER stability measurement of Pt_1/WC_x/CNTs and the Pt/C catalyst. Inset: LSV polarization curves before and after aging test. XPS spectra of (d) W 4f and (**e**) Pt 4f of Pt_1/WC_x@CNTs before and after the aging test. TEM image (f) and corresponding elemental mapping images (g–j) of Pt_1/WC_x@CNTs after aging test. (k) Comparison of operation time with reported HER catalysts.

extensive experimental evidence, including AC-HAADF-STEM imaging, EXAFS analysis, and the corresponding fitting results (Figure 4d and Table S3), the atomic configuration of Pt_1 on the WC_x carrier is defined as a Pt atom substituting the W atom and coordinating with surrounding C and W atoms, forming the atomically dispersed Pt_1/WC_x catalyst (inset in Figures 4d, S30, S31).

The calculated charge density difference (Figure 4e,f) of the Pt_1/WC_x hybrid demonstrates distinct charge delocalization and redistribution between atomic Pt and W atoms. The Pt incorporation induces the electron transfer from the tungsten carbide to the Pt center. Figure 4g provides the projected density of states (PDOSs) of pure WC_x and Pt_1/WC_x. The PDOSs of Pt-d do not have a significant contribution value because of the ultralow loading of a single Pt atom, whereas it can still alter the W-d and total PDOSs. Concurrently, the calculated Gibbs free energy of H* adsorption (ΔG_{H^*}) in Figure 4h exhibits a ΔG_{H^*} value of −0.54 eV for pure WC_x. In striking contrast, Pt_1/W_2C shows a ΔG_{H^*} value of−0.04 eV, which is closer to zero and comparable to that of bulk Pt (111), indicating the high intrinsic activity of Pt_1/W_2C.[35] This is mainly due to the strong metal–support interaction between the atomic Pt center and the tungsten carbide carrier. The introduction of single-atom Pt in tungsten carbide not only

https://doi.org/10.1021/acs.nanolett.4c05097
Nano Lett. XXXX, XXX, XXX−XXX

optimizes the charge distribution in Pt−W_2C interface, but also improves the H adsorption/desorption behavior, which synergistically promotes the HER thermodynamics and kinetics, leading to its high overall performance.[53,54] To verify this, the desorption of underpotential deposited hydrogen (H_{upd}) of different catalysts was conducted to evaluate the hydrogen binding energy (HBE). As shown in Figure 4i, the H_{upd} peak of Pt_1/WC_x@CNTs (0.048 V) is negative to that of WC_x@CNTs (0.082 V), indicating a weaker HBE due to the strong Pt_1−W_2C interaction, which is helpful for H recombination in the HER process.[36,38]

Long-Term Durability and Stability. We conducted the oxidation decay experiments at a potential of 1.2 V (Figure 5a). The current decays of WC_x@CNTs and WC_x/CNTs are over 50%, implying severe surface oxidation for pure carbides. In contrast, Pt_1/WC_x@CNTs demonstrate a much lower current decay of 10.3%, indicating most of the isolated Pt catalytic centers are preserved. The long-term durability of Pt_1/WC_x@CNTs, Pt_1/WC_x/CNTs, and Pt/C were evaluated by chronopotentiometry tests at a current density of 10 mA cm^{-2}. Compared with the commercial Pt/C catalyst and Pt_1/WC_x/CNTs, the Pt_1/WC_x@CNTs achieve more excellent stability over 500 h with a high current density retention up to 95.2% (Figures 5b,c and S32). These results demonstrate that the CNT encapsulation effectively enhances its catalytic stability, and the encapsulation of Pt_1/WC_x in nanotubes provides a potential armor to avoid structure degradation during the catalytic reactions.

Furthermore, we characterized the catalysts after an aging test. The W 4f and Pt 4f spectra (Figure 5d,e) of Pt_1/WC_x@CNT catalyst are almost consistent with the initial profiles, indicating that there are no significant changes in the valence state and coordination environment of W and Pt species. However, severe oxidation is observed for the carbide substrate of the Pt_1/WC_x/CNTs catalyst (Figure S33). The HRTEM image of the Pt_1/WC_x@CNTs after durability measurement shows the persistence of the structure (Figure 5f), where Pt_1/WC_x are still confined within the nanotube cavity, and the EDS elemental mapping shows the uniform dispersion of W and Pt elements inside the CNTs (Figures 5g−j). These analyses confirm the robust and stable structure of the Pt_1/WC_x@CNT catalyst.

Lastly, the stability of such chainmail catalysts is compared with other reports. As shown in Figure 5k and Table S4, the continuous operation time of our Pt_1/WC_x@CNTs is much longer than others at 10 mA cm^{-2}, evidencing the long-term stability of the designed Pt_1/WC_x@CNT chainmail catalyst. Overall, the stability of Pt_1/WC_x@CNTs can be ascribed to the strong metal−support (Pt-carbide) interactions with robust coordination and the nanoconfinement effect of MWCNTs, which can effectively protect the inner carbides from chemical degradation in acidic HER.

We propose an efficient and robust chainmail catalyst of Pt_1/WC_x@CNT, which is prepared by the CFJH method in less than 1 s. The carbothermal reduction reaction triggers the transition of polyoxometalates into well-defined WC_x carriers anchored with Pt atoms inside carbon nanotubes. The strong metal−support interaction of Pt_1/WC_x induces stabilization and activation of Pt atoms on the WC_x carrier, thus achieving greatly enhanced HER activity: the single-site Pt_1/WC_x@CNT catalyst demonstrates a low overpotential of 45.2 mV at 10 mA cm^{-2} in an acidic environment. The mass activity and TOF values are 9.01 A mg_{Pt}^{-1} and 9.17 s^{-1} at 150 mV, respectively, which are ∼3.9 times higher than that of the commercial Pt/C catalyst benchmark. The nanoconfinement of CNT chainmails endows high stability for the encapsulated Pt_1/WC_x nanocrystallites during a long-term durability test over 500 h. This work not only achieves rapid chainmail catalyst preparation with high intrinsic activity and durability, but also proposes a unique structure design. We envision broad applicability of the CFJH technique in the ultrafast and structure-controllable synthesis field by utilizing the high instantaneous temperature, rapid heating/cooling rate, and nanoconfinement effect.

■ ASSOCIATED CONTENT

Supporting Information

The Supporting Information is available free of charge at https://pubs.acs.org/doi/10.1021/acs.nanolett.4c05097.

Experimental details, characterizations, electrochemical analyses, and computational simulations (PDF)

■ AUTHOR INFORMATION

Corresponding Authors

Sheng Zhu − *Institute of Molecular Science, Key Laboratory of Chemical Biology and Molecular Engineering of Education Ministry, Shanxi University, Taiyuan 030006, China; Institute for Carbon-Based Thin Film Electronics, Peking University, Shanxi (ICTFE-PKU), Taiyuan 030012, China;* orcid.org/0000-0003-1713-0621; Email: shengzhu@sxu.edu.cn

Bing Deng − *School of Environment, Tsinghua University, Beijing 100084, China;* orcid.org/0000-0003-0530-8410; Email: dengbing@tsinghua.edu.cn

Authors

Qian Xu − *Institute of Molecular Science, Key Laboratory of Chemical Biology and Molecular Engineering of Education Ministry, Shanxi University, Taiyuan 030006, China*

Chong Guan − *Institute of Molecular Science, Key Laboratory of Chemical Biology and Molecular Engineering of Education Ministry, Shanxi University, Taiyuan 030006, China*

Yunzhen Chang − *Institute of Molecular Science, Key Laboratory of Chemical Biology and Molecular Engineering of Education Ministry, Shanxi University, Taiyuan 030006, China*

Gaoyi Han − *Institute of Molecular Science, Key Laboratory of Chemical Biology and Molecular Engineering of Education Ministry, Shanxi University, Taiyuan 030006, China; Institute for Carbon-Based Thin Film Electronics, Peking University, Shanxi (ICTFE-PKU), Taiyuan 030012, China;* orcid.org/0000-0002-7019-3392

Complete contact information is available at: https://pubs.acs.org/10.1021/acs.nanolett.4c05097

Author Contributions

S.Z. contributed to the idea and supervised the research. Q.X. performed the catalyst preparation and catalytic reaction test. Q.X., C.G., and Y.C. performed the material characterization. G.H., B.D., and S.Z. analyzed the data. Q.X. wrote the manuscript. B.D. and S.Z. revised the manuscript. All authors discussed the results and approved the manuscript.

Notes

The authors declare no competing financial interest.

https://doi.org/10.1021/acs.nanolett.4c05097
Nano Lett. XXXX, XXX, XXX−XXX

■ ACKNOWLEDGMENTS

This work was financially supported by the National Natural Science Foundation of China (52402284 and 92475112), Fundamental Research Program of Shanxi Province (202103021223019), Science and Technology Major Project of Shanxi (202101030201022), and startup fund of THU.

■ REFERENCES

(1) Xie, H.; Zhao, Z.; Liu, T.; Wu, Y.; Lan, C.; Jiang, W.; Zhu, L.; Wang, Y.; Yang, D.; Shao, Z. A membrane-based seawater electrolyser for hydrogen generation. *Nature* **2022**, *612*, 673−678.
(2) Wang, K.; Zhou, J.; Sun, M.; Lin, F.; Huang, B.; Lv, F.; Zeng, L.; Zhang, Q.; Gu, L.; Luo, M.; et al. Cu-doped heterointerfaced Ru/$RuSe_2$ nanosheets with optimized H and H_2O adsorption boost hydrogen evolution catalysis. *Adv. Mater.* **2023**, *35*, 2300980.
(3) Cui, X.; Liu, Y.; Chen, Y. Ultrafast micro/nano-manufacturing of metastable materials for energy. *Natl. Sci. Rev.* **2024**, *11*, No. nwae033.
(4) Ahmadi Khoshooei, M.; Wang, X.; Vitale, G.; Formalik, F.; Kirlikovali, K. O.; Snurr, R. Q.; Pereira-Almao, P.; Farha, O. K. An active, stable cubic molybdenum carbide catalyst for the high-temperature reverse water-gas shift reaction. *Science* **2024**, *384*, 540−546.
(5) Quan, L.; Chen, X.; Liu, J.; Fan, S.; Xia, B.; You, B. Atomic Pt-N_4 sites in porous N-doped nanocarbons for enhanced on-site chlorination coupled with H_2 evolution in acidic water. *Adv. Funct. Mater.* **2023**, *33*, 2307643.
(6) Dai, L.; Chen, Z.; Li, L.; Yin, P.; Liu, Z.; Zhang, H. Ultrathin Ni (0)-embedded $Ni(OH)_2$ heterostructured nanosheets with enhanced electrochemical overall water splitting. *Adv. Mater.* **2020**, *32*, 1906915.
(7) Yao, S.; Zhang, X.; Zhou, W.; Gao, R.; Xu, W.; Ye, Y.; Lin, L.; Wen, X.; Liu, P.; Chen, B.; et al. Atomic-layered Au clusters on α-MoC as catalysts for the low-temperature water-gas shift reaction. *Science* **2017**, *357*, 389−393.
(8) Wang, Z.; Li, M.; Yu, J.; Ge, X.; Liu, Y.; Wang, W. Low-iridium-content IrNiTa metallic glass films as intrinsically active catalysts for hydrogen evolution reaction. *Adv. Mater.* **2020**, *32*, 1906384.
(9) Ge, Y.; Qin, X.; Li, A.; Deng, Y.; Lin, L.; Zhang, M.; Yu, Q.; Li, S.; Peng, M.; Xu, Y.; et al. Maximizing the Synergistic Effect of CoNi Catalyst on α-MoC for Robust Hydrogen Production. *J. Am. Chem. Soc.* **2021**, *143*, 628−633.
(10) Liu, S.; Li, H.; Zhong, J.; Xu, K.; Wu, G.; Liu, C.; Zhou, B.; Yan, Y.; Li, L.; Cha, W.; et al. A crystal glass-nanostructured Al-based electrocatalyst for hydrogen evolution reaction. *Sci.Adv.* **2022**, *8*, No. eadd6421.
(11) Li, C.; Wang, Z.; Liu, M.; Wang, E.; Wang, B.; Xu, L.; Jiang, K.; Fan, S.; Sun, Y.; Li, J.; et al. Ultrafast self-heating synthesis of robust heterogeneous nanocarbides for high current density hydrogen evolution reaction. *Nat. Commun.* **2022**, *13*, 3338.
(12) Wu, J.; Su, J.; Wu, T.; Huang, L.; Li, Q.; Luo, Y.; Jin, H.; Zhou, J.; Zhai, T.; Wang, D.; et al. Scalable synthesis of 2D Mo_2C and thickness-dependent hydrogen evolution on its basal plane and edges. *Adv. Mater.* **2023**, *35*, 2209954.
(13) Lin, L.; Yu, Q.; Peng, M.; Yao, S.; Tian, S.; Liu, X.; Li, A.; Jiang, Z.; Gao, R.; Han, X.; et al. Atomically dispersed Ni/α-MoC catalyst for hydrogen production from methanol/water. *J. Am. Chem. Soc.* **2021**, *143*, 309−317.
(14) Chen, Z.; Li, L.; Chu, Y.; Zhao, F.; Zhu, Y.; Tong, S.; Zheng, H. Bio-inspired superhydrophilic self-assembled coronavirus-like Pt-WC/CNT for hydrogen evolution reaction. *Small* **2024**, *20*, 2309675.
(15) Yang, Y.; Qian, Y.; Li, H.; Zhang, Z.; Mu, Y.; Do, D.; Zhou, B.; Dong, J.; Yan, W.; Qin, Y.; et al. O-coordinated W-Mo dual-atom catalyst for pH-universal electrocatalytic hydrogen evolution. *Sci. Adv.* **2020**, *6*, No. eaba6586.
(16) Gao, X.; Dai, Q.; Lu, X.; Kawi, S. Carbon-supported non-noble metal single-atom catalysts for electro-catalytic hydrogen evolution reaction. *Int. J. Hydrogen Energy* **2023**, *48*, 17106−17136.
(17) Wu, L.; Zhang, F.; Song, S.; Ning, M.; Zhu, Q.; Zhou, J.; Gao, G.; Chen, Z.; Zhou, Q.; Xing, X.; et al. Efficient alkaline water/seawater hydrogen evolution by a nanorod-nanoparticle-structured Ni-MoN catalyst with fast water-dissociation kinetics. *Adv. Mater.* **2022**, *34*, 2201774.
(18) Ma, R.; Song, E.; Zhou, Y.; Zhou, Z.; Liu, G.; Liu, Q.; Liu, J.; Zhu, Y.; Wang, J. Ultrafine WC nanoparticles anchored on co-encased, N-doped carbon nanotubes for efficient hydrogen evolution. *Energy Storage Mater.* **2017**, *6*, 104−111.
(19) Diao, J.; Qiu, Y.; Liu, S.; Wang, W.; Chen, K.; Li, H.; Yuan, W.; Qu, Y.; Guo, X. Interfacial engineering of W_2N/WC heterostructures derived from solid-state synthesis: a highly efficient trifunctional electrocatalyst for ORR, OER, and HER. *Adv. Mater.* **2020**, *32*, 1905679.
(20) Ouyang, T.; Ye, Y.; Wu, C.; Xiao, K.; Liu, Z. Heterostructures composed of n-doped carbon nanotubes encapsulating cobalt and β-Mo_2C nanoparticles as bifunctional electrodes for water splitting. *Angew. Chem., Int. Ed.* **2019**, *58*, 4923−4928.
(21) Kim, M.; Kim, Y.; Ha, M.; Shin, E.; Kwak, S.; Park, M.; Kim, I.; Jung, W.; Lee, W.; Kim, Y.; et al. Exploring optimal water splitting bifunctional alloy catalyst by pareto active learning. *Adv. Mater.* **2023**, *35*, 2211497.
(22) Li, J.; Wang, C.; Chen, X.; Zhang, Y.; Zhang, Y.; Fan, K.; Zong, L.; Wang, L. Flash synthesis of ultrafine and active NiRu alloy nanoparticles on N-rich carbon nanotubes via joule heating for efficient hydrogen and oxygen evolution reaction. *J. Alloys Compd.* **2023**, *959*, 170571.
(23) Muravev, V.; Parastaev, A.; van den Bosch, Y.; Ligt, B.; Claes, N.; Bals, S.; Kosinov, N.; Hensen, E. J. M. Size of cerium dioxide support nanocrystals dictates reactivity of highly dispersed palladium catalysts. *Science* **2023**, *380*, 1174−1178.
(24) Ramalingam, V.; Varadhan, P.; Fu, H.; Kim, H.; Zhang, D.; Chen, S.; Song, L.; Ma, D.; Wang, Y.; Alshareef, H.; et al. Heteroatom-mediated interactions between ruthenium single atoms and an MXene support for efficient hydrogen evolution. *Adv. Mater.* **2019**, *31*, 1903841.
(25) Zhu, Y.; Fan, K.; Hsu, C.; Chen, G.; Chen, C.; Liu, T.; Lin, Z.; She, S.; Li, L.; Zhou, H.; et al. Supported ruthenium single-atom and clustered catalysts outperform benchmark Pt for alkaline hydrogen evolution. *Adv. Mater.* **2023**, *35*, 2301133.
(26) Zhou, K.; Wang, Z.; Han, C.; Ke, X.; Wang, C.; Jin, Y.; Zhang, Q.; Liu, J.; Wang, H.; Yan, H. Platinum single-atom catalyst coupled with transition metal/metal oxide heterostructure for accelerating alkaline hydrogen evolution reaction. *Nat. Commun.* **2021**, *12*, 3783.
(27) Zhang, Z.; Liu, J.; Wang, J.; Wang, Q.; Wang, Y.; Wang, K.; Wang, Z.; Gu, M.; Tang, Z.; Lim, J.; et al. Single-atom catalyst for high-performance methanol oxidation. *Nat. Commun.* **2021**, *12*, 5235.
(28) Li, H.; Wang, L.; Dai, Y.; Pu, Z.; Lao, Z.; Chen, Y.; Wang, M.; Zheng, X.; Zhu, J.; Zhang, W.; et al. Synergetic interaction between neighbouring platinum monomers in CO_2 hydrogenation. *Nat. Nanotechnol.* **2018**, *13*, 411−417.
(29) Shi, Z.; Zhang, X.; Lin, X.; Liu, G.; Ling, C.; Xi, S.; Chen, B.; Ge, Y.; Tan, C.; Lai, Z.; et al. Phase-dependent growth of Pt on MoS_2 for highly efficient H_2 evolution. *Nature* **2023**, *621*, 300−305.
(30) Pu, Z.; Amiinu, I.; Kou, Z.; Li, W.; Mu, S. RuP_2-based catalysts with platinum-like activity and higher durability for the hydrogen evolution reaction at all pH values. *Angew. Chem., Int. Ed.* **2017**, *129*, 11717−11722.
(31) Wang, W.; Wu, Y.; Lin, Y.; Yao, J.; Wu, X.; Wu, C.; Zuo, X.; Yang, Q.; Ge, B.; Yang, L.; et al. Confining zero-valent platinum single atoms in α-MoC_{1-x} for pH-universal hydrogen evolution reaction. *Adv. Funct. Mater.* **2022**, *32*, 2108464.
(32) Zhang, H.; Wu, F.; Huang, R.; Liu, X.; Zhang, Z.; Yao, T.; Zhang, Y.; Wu, Y. Symmetry evolution induced 2D Pt single atom catalyst with high density for alkaline hydrogen oxidation. *Adv. Mater.* **2024**, *36*, 2404672.
(33) He, T.; Wang, W.; Shi, F.; Yang, X.; Li, X.; Wu, J.; Yin, Y.; Jin, M. Mastering the surface strain of platinum catalysts for efficient electrocatalysis. *Nature* **2021**, *598*, 76−81.

https://doi.org/10.1021/acs.nanolett.4c05097
Nano Lett. XXXX, XXX, XXX−XXX

(34) Yang, W.; Zhao, X.; Wang, Y.; Wang, R.; Yang, W.; Peng, Y.; Li, J. Selective dissolution to synthesize densely populated Pt single atom catalyst. *Nano Res.* **2023**, *16*, 219−227.
(35) Ma, T.; Cao, H.; Li, S.; Cao, S.; Zhao, Z.; Wu, Z.; Yan, R.; Yang, C.; Wang, Y.; Aken, P.; et al. Electronic structures and hydrogen evolution. *Adv. Mater.* **2022**, *34*, 2206368.
(36) Wang, L.; Xu, Z.; Kuo, C.; Peng, J.; Hu, F.; Li, L.; Chen, H.; Wang, J.; Peng, S. Stabilizing low-valence single atoms by constructing metalloid tungsten carbide supports for efficient hydrogen oxidation and evolution. *Angew. Chem., Int. Ed.* **2023**, *135*, No. e202311937.
(37) Li, S.; Chen, B.; Wang, Y.; Ye, M.; van Aken, P.; Cheng, C.; Thomas, A. Oxygen-evolving catalytic atoms on metal carbides. *Nat. Mater.* **2021**, *20*, 1240−1247.
(38) Lin, X.; Hu, W.; Xu, J.; Liu, X.; Jiang, W.; Ma, X.; He, D.; Wang, Z.; Li, W.; Yang, M.; et al. Alleviating OH blockage on the catalyst surface by the puncture effect of single-atom sites to boost alkaline water electrolysis. *J. Am. Chem. Soc.* **2024**, *146*, 4883−4891.
(39) Wang, K.; Xia, G.; Liu, T.; Yun, Y.; Wang, W.; Cao, K.; Yao, F.; Zhao, X.; Yu, B.; Wang, Y.; et al. Anisotropic growth of one-dimensional carbides in single-walled carbon nanotubes with strong interaction for catalysis. *J. Am. Chem. Soc.* **2023**, *145*, 12760−12770.
(40) Chen, Y.; Egan, G.; Wan, J.; Zhu, S.; Jacob, R. J.; Zhou, W.; Dai, J.; Wang, Y.; Danner, V.; Yao, Y.; et al. Ultra-fast self-assembly and stabilization of reactive nanoparticles in reduced graphene oxide films. *Nat. Commun.* **2016**, *7*, 12332.
(41) Zeng, C.; Duan, C.; Guo, Z.; Liu, Z.; Dou, S.; Yuan, Q.; Liu, P.; Zhang, J.; Luo, J.; Liu, W.; et al. Ultrafastly activated needle coke as electrode material for supercapacitors. *Prog. Nat. Sci. Mater. Int.* **2022**, *32*, 786−792.
(42) Zhu, S.; Ding, L.; Zhang, X.; Wang, K.; Wang, X.; Yang, F.; Han, G. Biaxially-strained phthalocyanine at polyoxometalate@carbon nanotube heterostructure boosts oxygen reduction catalysis. *Angew. Chem., Int. Ed.* **2023**, *62*, No. e202309545.
(43) Deng, B.; Wang, Z.; Choi, C. H.; Li, G.; Yuan, Z.; Chen, J.; Luong, D. X.; Eddy, L.; Shin, B.; Lathem, A.; et al. Kinetically Controlled Synthesis of Metallic Glass Nanoparticles with Expanded Composition Space. *Adv. Mater.* **2024**, *36*, 2309956.
(44) Li, H.; Wang, W.; Xue, S.; He, J.; Liu, C.; Gao, G.; Di, S.; Wang, S.; Wang, J.; Yu, Z.; et al. Superstructure-assisted single-atom catalysis on tungsten carbides for bifunctional oxygen reactions. *J. Am. Chem. Soc.* **2024**, *146*, 9124−9133.
(45) Shanenkov, I.; Ivashutenko, A.; Shanenkova, Y.; Nikitin, D.; Zhu, Y.; Li, J.; Han, W.; Sivkov, A. Composite material WC_{1-x}@C as a noble-metal-economic material for hydrogen evolution reaction. *J. Alloys Compd.* **2020**, *834*, 155116.
(46) Qin, G.; Sun, S.; Zhang, X.; Han, Z.; Li, Y.; Han, G.; Li, Y.; Zhu, S. Millisecond activity modulation of atomically-dispersed Fe−N−C catalysts. *Energy Storage Mater.* **2024**, *69*, 103421.
(47) Pakharukov, I. Y.; Prosvirin, I. P.; Chetyrin, I. A.; Bukhtiyarov, V. I.; Parmon, V. N. In situ XPS studies of kinetic hysteresis in methane oxidation over Pt/γ-Al_2O_3 catalysts. *Catal. Today* **2016**, *278*, 135−139.
(48) Zhang, H.; An, P.; Zhou, W.; Guan, B. Y.; Zhang, P.; Dong, J.; Lou, X. W. Dynamic traction of lattice-confined platinum atoms into mesoporous carbon matrix for hydrogen evolution reaction. *Sci. Adv.* **2018**, *4*, No. eaao6657.
(49) Li, X.; Pereira-Hernández, X. I.; Chen, Y.; Xu, J.; Zhao, J.; Pao, C.-W.; Fang, C.-Y.; Zeng, J.; Wang, Y.; Gates, B. C.; et al. Functional CeO_x nanoglues for robust atomically dispersed catalysts. *Nature* **2022**, *611*, 284−288.
(50) Zhang, T.; Yang, X.; Jin, J.; Han, X.; Fang, Y.; Zhou, X.; Li, Y.; Han, A.; Wang, Y.; Liu, J. Modulating the electronic metal-support interactions to anti-leaching Pt single atoms for efficient hydrosilylation. *Adv. Mater.* **2024**, *36*, 2304144.
(51) Kang, Y.; Li, S.; Cretu, O.; Kimoto, K.; Zhao, Y.; Zhu, L.; Wei, X.; Fu, L.; Jiang, D.; Wan, C.; et al. Mesoporous amorphous non-noble metals as versatile substrates for high loading and uniform dispersion of Pt- group single atoms. *Sci. Adv.* **2024**, *10*, No. eado2442.
(52) Zhang, E.; Dong, A.; Yin, K.; Ye, C.; Zhou, Y.; Tan, C.; Li, M.; Zheng, X.; Wang, Y.; Gao, X.; et al. Electron localization in rationally designed Pt_1Pd single-atom alloy catalyst enables high-performance Li−O_2 batteries. *J. Am. Chem. Soc.* **2024**, *146*, 2339−2344.
(53) Zhang, X.; Zhang, M.; Deng, Y.; Xu, M.; Artiglia, L.; Wen, W.; Gao, R.; Chen, B.; Yao, S.; Zhang, X.; et al. A stable low-temperature H_2-production catalyst by crowding Pt on α-MoC. *Nature* **2021**, *589*, 396−401.
(54) Lin, L.; Zhou, W.; Gao, R.; Yao, S.; Zhang, X.; Xu, W.; Zheng, S.; Jiang, Z.; Yu, Q.; Li, Y.-W.; et al. Low-temperature hydrogen production from water and methanol using Pt/α-MoC catalysts. *Nature* **2017**, *544*, 80−83.

https://doi.org/10.1021/acs.nanolett.4c05097
Nano Lett. XXXX, XXX, XXX−XXX